

Comparison of bolus- and filtering-based EIT measures of lung perfusion in an animal model

Symon Stowe^{1*}, Alistair Boyle¹, Michaël Sage², Wendy See²,
Jean-Paul Praud², Étienne Fortin-Pellerin², Andy Adler¹

¹Systems and Computer Engineering, Carleton University, Ottawa, Canada

²Department of Paediatrics and Pharmacology/Physiology, Université de Sherbrooke, Québec, Canada

E-mail: *Corresponding author: Email: symonstowe@sce.carleton.ca

Abstract. *Objective:* Two main functional imaging approaches have been used to measure regional lung perfusion using Electrical Impedance Tomography (EIT): venous injection of a hypertonic saline contrast agent and imaging of its passage through the heart and lungs, and digital filtering of heart-frequency impedance changes over sequences of EIT images. This paper systematically compares filtering-based perfusion estimates and bolus injection methods to determine to which degree they are related. *Approach:* EIT data was recorded on 7 mechanically ventilated newborn lambs in which ventilation distribution was varied through changes in posture between prone, supine, left- and right-lateral positions. Perfusion images were calculated using frequency filtering and ensemble averaging during both ventilation and apnoea time segments for each posture to compare against contrast agent-based methods using Jaccard distance score. *Main Results:* Using bolus-based EIT measures of lung perfusion as the reference frequency filtering techniques performed better than ensemble averaging and both techniques performed equally well across apnoea and ventilation data segments. *Significance:* Our results indicate the potential for use of filtering-based EIT measures of heart-frequency activity as a non-invasive proxy for contrast agent injection-based measures of lung perfusion.

1. Introduction

Electrical Impedance Tomography (EIT) uses electrical stimulation and measurements at electrodes on the body surface to reconstruct images of internal conductivity distribution and its changes. The most common application of EIT, experimentally and clinically, has been for imaging of the thorax (Frerichs *et al.* 2017). Using a ring of electrodes around the chest, EIT is able to calculate images of impedance changes in the abdomen. Although most research has focused on imaging of ventilation, there is significant interest in imaging cardiovascular phenomena with EIT (Adler *et al.* 2012; Leonhardt *et al.* 2012).

EIT has been evaluated for its ability to measure cardiac output and lung perfusion since the early 90s (Eyüboğlu *et al.* 1989; Frerichs *et al.* 2002; Zadehkoochak *et al.*

1992). Since then, various configurations of EIT have been evaluated (Borges *et al.* 2012; Nguyen *et al.* 2015). The effect of posture on EIT images was evaluated by Reifferscheid *et al.* (2011), who showed that changing posture introduces a large and reproducible variability into ventilation distribution as imaged by EIT. Based on results showing a common relationship between the effect of gravity and perfusion in both children and adults (Bhuyan *et al.* 1989), in newborns we expect to see a comparable directional change in perfusion due to the changes in posture. Recently, Braun *et al.* (2018) evaluated EIT's ability to monitor cardiac output, showing that EIT is more reliable for monitoring cardiac output trends than absolute cardiac output. EIT has also been investigated for monitoring of systemic blood pressure (Solà *et al.* 2011), and for monitoring of pulmonary arterial pressure (Proença *et al.* 2017).

EIT measurements are sensitive to blood movement in two main ways. First, it is possible to image the transit of the contrast agent through the heart and lungs via a conductivity-contrasting bolus into the veins and second, through digital filtering of the time series of EIT images at the heart frequency (Leathard *et al.* 1994). While multiple EIT measures of perfusion are used, their relationship is not well understood. It is currently unclear to what degree pulsatile impedance changes represent blood flow, and how they limit the potential for heart-frequency filtering to correctly estimate the true perfusion (Nguyen *et al.* 2012).

Injection of a contrast agent to measure regional lung perfusion has been compared with electron beam computed tomography (EBCT) and determined to be feasible for measuring perfusion across different animals (Frerichs *et al.* 2002). Perfusion measurement via conductivity contrasts has the advantage of measuring the true perfusion, but requires placement of a catheter to introduce the contrast agent. Bolus-derived measurements cannot be made continuously because they rely upon the circulation of a contrast agent. In addition, the accumulation of NaCl (the main conductivity contrast used) over multiple injections can lead to hypernatremia which limits the rate at which bolus injections can be made.

Calculating the heart-frequency conductivity changes in the thorax offers the benefit of a continuous functional measure calculated directly from EIT signals (possibly in conjunction with a synchronization signal such as the ECG). Heart-frequency EIT signals are typically an order of magnitude smaller than ventilation signals; thus, when measurements are made during tidal ventilation, a large period of data must be used in order to reduce the ventilation signal. On the other hand, measurements during apnoea can be used to eliminate the ventilation signal, but for the safety of the patient the apnoea was limited to 30 s. In healthy human subject of less than one year old it takes a mean of 118 s for the blood oxygen saturation levels to drop below 90% (Xue *et al.* 1996), however the length of safe apnoea is much shorter for the sick preterm infant. The time period was chosen based on experience in the lab showing that 30 s seconds was not associated with bradycardia or desaturation to less than 90% blood oxygen saturation.

There is a debate within the EIT community about the meaning of heart-frequency

EIT signals (Adler *et al.* 2017a; Frerichs *et al.* 2017). Not all perfusion results in a cardiac-frequency change (for example, continuous blood flow in capillaries), and non-perfusion effects (for example, heart movement in the thoracic cavity) can result in heart-frequency EIT signals. This debate is reflected by the terminology – perfusion vs. pulsatility. Those who prefer “pulsatility” or “heart-frequency fEIT image” seek to emphasise that frequency filtered signals are not “perfusion” (although they may be related). While these pulsatility based EIT images are clearly not a direct measure of perfusion, the signals appear to be useful and are often measured and reported (Bartocci *et al.* 1999; Ericsson *et al.* 2016; Halter *et al.* 2008; Moens *et al.* 2014). To the authors’ knowledge, no systematic comparison of frequency-based perfusion measures has been published.

The heart-frequency signal can be derived from frequency filtering or ensemble averaging. Frequency-filtering uses a filter to isolate the frequency of heart-frequency conductivity changes, and was introduced by Zadehkoochak *et al.* (1992) and Leathard *et al.* (1994). Frequency filtering is susceptible to interference from ventilation when the heart rate is at a harmonic of the breathing rate. Ensemble averaging is another filtering approach which averages signals at a synchronized time, for example at the QRS peak (Bartocci *et al.* 1999; Deibebe *et al.* 2008). The impedance change due to each heart beat is aligned and averaged to give a single heart-related impedance change, representative of all heart-beats in the segment.

In this paper, we are motivated to better understand the relationship between lung perfusion and heart-frequency filtering measures, and between the various filtering approaches used to determine heart-frequency components. Our questions are: 1) to what extent do heart-frequency filtering-based measures correspond to perfusion, 2) what are the advantages and disadvantages of different approaches to heart-frequency filtering of EIT data, and 3) which techniques are recommended. In our experimental protocol, we have selected posture-change to introduce changes in the regional distribution of lung perfusion. These changes are then compared using bolus- and filtering-based EIT measures.

2. Methods

2.1. Overview

Data were acquired as an additional protocol within a study to determine a baseline for lung damage due to gas ventilation in neonatal lambs. This is part of an effort to establish total liquid ventilation (TLV) as a less-injurious ventilation strategy for the delicate lungs of neonatal subjects (Sage *et al.* 2018). In order to induce changes in ventilation and perfusion patterns, posture changes were made between supine, prone, left and right lateral positions.

2.2. Animals

The study was conducted in accordance with the Canadian Council on Animal Care guidelines upon approval by the animal research ethics board of Université de Sherbrooke (protocol 417-17BR).

Seven healthy neonatal lambs (2–4 days old and 2.95 ± 0.27 kg) were used. Animals were anaesthetised (ketamin 10 mg/kg IM at induction followed by propofol 100 mcg/kg/min and ketamin 2 mg/kg/h IV) and placed under mechanical gas ventilation with: peak inspiratory pressure (PIP) 15 cmH₂O, positive end-expiratory pressure (PEEP) 5 cmH₂O, respiratory rate (RR) of 60/min, and fractional concentration of O₂ in inspired gas (FiO₂) of 30%.

A catheter was inserted into the carotid artery for blood gas and continuous blood pressure monitoring. A jugular venous access was inserted to inject the saline bolus for generating perfusion images. Each animal was shaved for placement of a custom EIT belt around the lower third of the sternum in the transverse plane.

For each animal a bolus injection protocol was used: 1.5 mL of 7.5% saline was injected into the jugular vein at a constant rate over approximately 2s. Before each bolus, ventilation was stopped for ten seconds, and a further twenty seconds of apnoea was maintained before restarting ventilation.

After one hour of ventilation (for stabilization) EIT recordings were made during the position change procedure. Each lamb was rotated onto its right side. Five minutes after turning the subject, the bolus injection protocol was implemented. The animal was then ventilated normally, remaining on the right side for an additional five minutes, before being positioned on the left side for 5 minutes of regular ventilation, followed by the bolus injection protocol.

At 2 hours of ventilation, the position change procedure was repeated, changing the positioning of the lamb from prone to supine as the bolus injection protocol was repeated and EIT recordings were captured.

2.3. Data Acquisition and Image Reconstruction

EIT data was acquired with the Pioneer Set (Swisstom, Landquart, Switzerland) using a custom electrode belt (at an acquisition rate of 20 frames/s). The belt uses 32 brass electrodes equally spaced around the thorax, using an ultrasound gel to ensure good contact and minimise the contact impedance. The selected data in this study comes from lateral positioning changes recorded after 1.5 hours of ventilation and prone to supine positioning changes after 2 hours.

EIT images were reconstructed using GREIT (Adler *et al.* 2009), which calculates a reconstruction matrix **R** from which the reconstructed image is calculated as $\hat{\mathbf{x}} = \mathbf{R}\mathbf{y}$, where **y** are the time-difference measurements, $\mathbf{y}(t) = \mathbf{v}(t) - \mathbf{v}(t_r)$, where **v**(t) represents the data frame acquired at time, *t*, and **v**(*t_r*) measurements acquired at a “reference” time, *t_r* in the case of this experiment the reference was a mean of 10 images preceding the bolus injection.

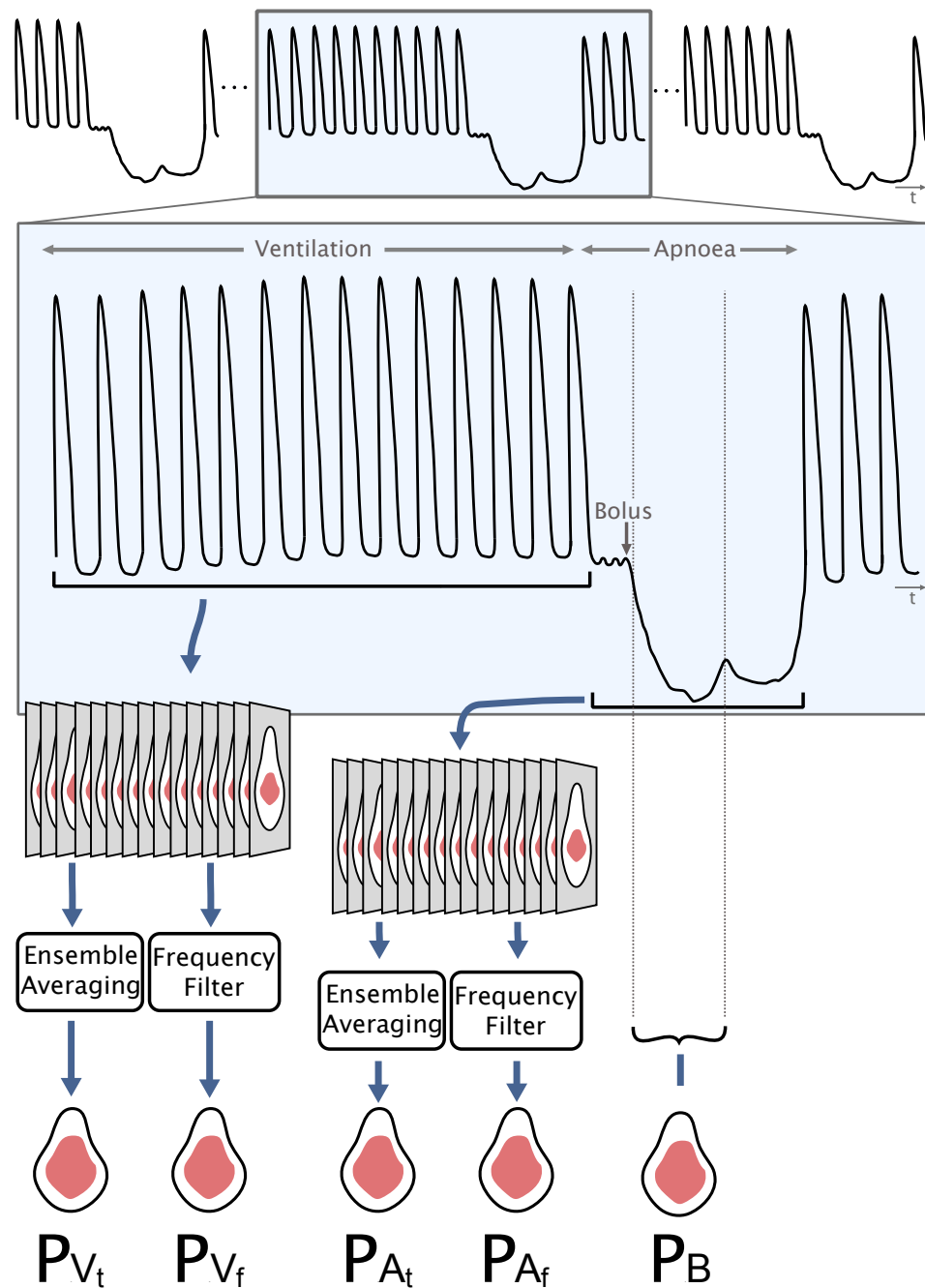


Figure 1. This figure is a schematic overview of analysis methods for EIT perfusion. The upper curve illustrates the global EIT signal during a period of ventilation followed by apnoea and renewed ventilation. During apnoea a bolus of conductivity contrasting saline is introduced. From these data 5 fEIT images are calculated: P_{Vt} : pulsatility (perfusion) image during ventilation, calculated by ensemble averaging EIT data during ventilation; P_{Vf} : pulsatility (perfusion) image during ventilation, calculated by frequency filtering EIT data during ventilation; P_{At} : pulsatility (perfusion) image during apnoea, calculated by ensemble averaging EIT data during apnoea; P_{Af} : pulsatility (perfusion) image during apnoea, calculated by frequency filtering EIT data during apnoea; P_B : perfusion image from bolus, calculated between a reference measure during apnoea and one during the bolus

The linear reconstruction matrix $\mathbf{R} = \mathbf{D}\boldsymbol{\Sigma}_t\mathbf{J}^T (\mathbf{J}\boldsymbol{\Sigma}_t\mathbf{J} + \boldsymbol{\Sigma}_n)^{-1}$ is calculated from a finite element model of the body and electrode geometry $F(\cdot)$ and covariance estimates of the image, $\boldsymbol{\Sigma}_t$, noise, $\boldsymbol{\Sigma}_n$ (Grychtol *et al.* 2016), and a spatial filtering matrix, \mathbf{D} .

EIT data from this experiment was prone to errors consisting of brief periods of zeroed measurements stemming from the synchronisation equipment. Measurements that were zeroed by the device were removed and replaced with linearly extrapolated data to allow for frequency-based analysis over all selected segments of data. A moving median filter with a width of 3 was used to further remove the noise caused by single measurement errors in the signal.

2.4. Functional EIT Images

In each animal 4 episodes were recorded — one in each posture — to generate 5 different functional EIT images.

The images Bolus-based measures of lung perfusion (P_B) were calculated using time-difference reconstructions. Heart-frequency filtering during ventilation (P_{Vf}) and apnoea (P_{Af}) used frequency analysis of EIT image sequences, as illustrated in figure 3, and ensemble averaging-based methods during ventilation P_{Vt} and apnoea P_{At} are calculated using ensemble averaging of identified pulsatile components figure 4.

The following methods were conducted on segments of data collected both during apnoea and ventilation. Apnoea regions were selected as the total time that ventilation was arrested, including the bolus section and had a duration of 30s. The ventilation data was selected as 30s of data immediately preceding the induction of apnoea. Regions of interest including lung, and heart areas in the images were defined by the lamb model provided in EIDORS (Adler *et al.* 2017b).

2.4.1. Bolus injection image (P_B) The beginning of the saline bolus injection was determined as the point immediately preceding the drop in impedance from the conductive agent, and is shown in figure 2 at the point marked “injection”. The mean of 10 images including and immediately preceding the bolus injection were used as the reference to which all bolus images were reconstructed from. To image perfusion, the point with maximum decline in impedance over the sum of the pixels in the lung region relative to the reference was selected based on the methods presented by Frerichs *et al.* (2002). In figure 2 this was found at the point marked “perfusion”. This method was used as the standard perfusion measuring technique against which the other methods were compared.

2.4.2. Frequency-Filtering Heart-frequency EIT images during the selected events were calculated by taking the FFT of the time-series image data after first applying a Blackman window: $w(n) = a_0 - a_1 \cos\left(\frac{2\pi n}{N-1}\right) + a_2 \cos\left(\frac{4\pi n}{N-1}\right)$ with $a_0 = 0.42$, $a_1 = 0.5$ and $a_2 = 0.08$, where N is the number of time-series EIT images in the selected event.

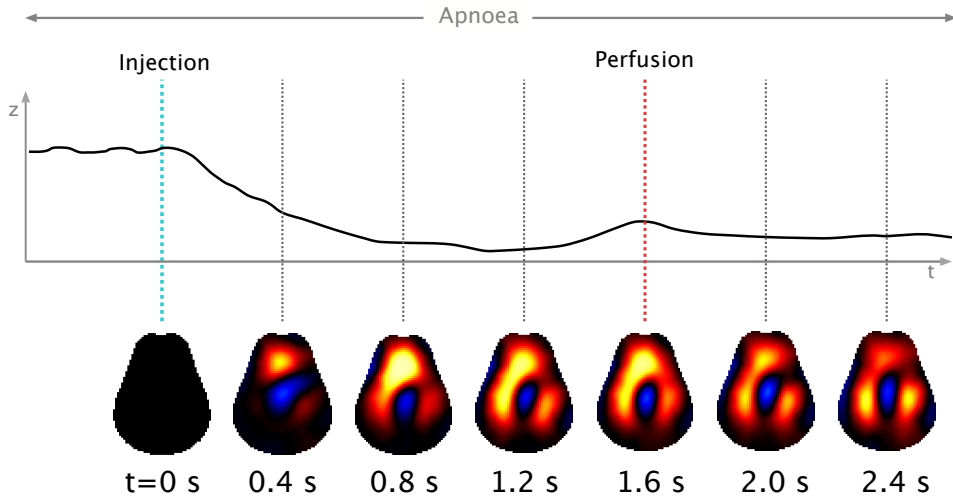


Figure 2. The method used to select the perfusion point from the bolus injection is shown in the figure above. The point with the widest spread of high conductivity was selected as the point of perfusion, shown here at 1.6 seconds after the contrast agent injection. The image series shows the conductivity contrast as the bolus injection travels through the thorax.

An FFT was calculated from a series of images restricted to pixels in the heart region. From the FFT of all pixels the heart region, the heart frequency was selected as the largest peak between 3 and 4.5 Hz, representing a heart rate between 180 and 240 bpm (typical for a newborn lamb).

The identified heart rate was used to select changes at the heart-frequency in the frequency domain images of the entire thorax. Images at 3 frequencies on either side of the heart rate were also reconstructed to account for changed in heart rate over the course of the data collection. A Blackman window with a length of 7 was applied surrounding the heart frequency to generate a weighted mean of the images, resulting in a single perfusion image from the heart-frequency data.

The output of the frequency filtering method is an image with complex values assigned to each pixel.

Depending on the timing of the pulsatility-based changes within the selected signal the real component of frequency analysed image did not correspond to the maximum conductivity change in the lungs in every event. In order to correct this, each image was displayed along the axis that gave the maximum real component contained within the lung region to ensure the maximum change in impedance related to pulsatile activity in the lungs was calculated.

2.4.3. Ensemble Averaging Time series data of the total impedance signal for each pixel in the heart region was filtered using a bandpass filter to eliminate noise and breathing changes, and allow the heartbeat to be seen clearly in the signal. Peak detection was used on this heart-region data to select the amplitude peaks in impedance change signal

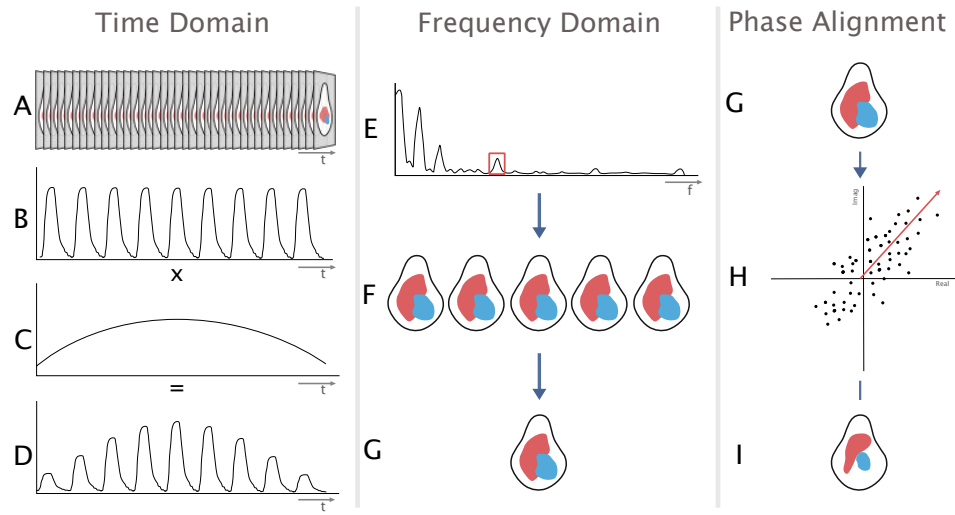


Figure 3. Frequency analysis methodology used for obtaining a perfusion image from the time series data. Steps are: A) to reconstruct the images from time series measurements; B) - D) window the time series data before performing a FFT on the data for each element; E) Select the dominant frequency between 3 and 4.5 Hz as the heart frequency; F) reconstruct the image at the heart frequency and selected nearby frequencies; G) take the mean of the images at the heart frequency using a Blackman window to give greater weight to those closer to the center; H) I) select the image that will give the maximum real component contained in the lung region.

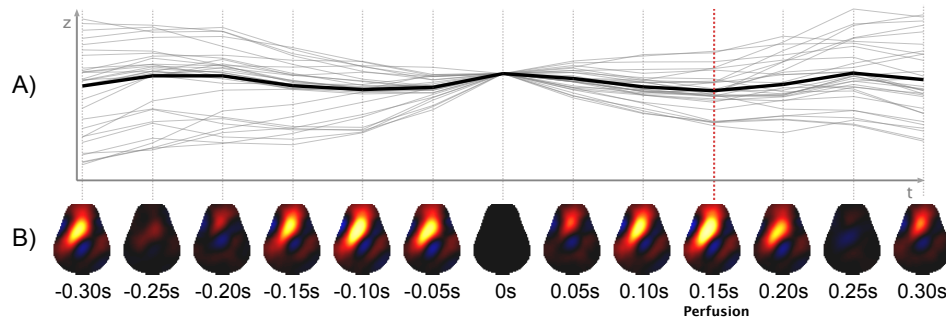


Figure 4. Illustration of the stages of the ensemble averaging process: A) an ensemble average of all heartbeats over the time frame is taken from the summed global signal; and B) shows reconstructed images corresponding to each time point in the global ensemble averaged signal above. The selected perfusion image is the image with the maximum impedance increase in the lung region.

at the heart frequency.

Using the identified time points, the global impedance change signal was ensemble averaged by overlaying all identified peaks to give an averaged heartbeat. 13 images were reconstructed over the course of the heart beat to select the image that resulted in the maximum positive increase impedance within the lung region. This process is outlined in figure 4.

2.5. Image Comparison

To compare the images the Jaccard distance between functional EIT images was calculated. Negative impedance changes were removed from the images and the images were normalized.

The Jaccard distance was calculated between the reference image calculated using the maximum increase in lung-region conductivity during bolus injection (b), and the frequency-based method (f): $J(x, y) = \sum_i \frac{\min(b_i, f_i)}{\max(b_i, f_i)}$ representing the distance between the two images.

2.6. Statistical Analysis

To determine the significance of the change in bolus between postures and methods, the Cohen's d score was calculated to quantify the effect size of the change in the centre of mass of the perfusion image (Cohen 1988). This was calculated as the difference between two means over the pooled standard deviation. Where the difference between the two means is: $\mu_1 - \mu_2$, and the pooled standard deviation is: $\sqrt{\frac{(n_1-1)s_1^2 + (n_2-1)s_2^2}{n_1+n_2-2}}$.

3. Results

The Jaccard scores for each method were compared between ensemble averaging and frequency filtering methods to determine the regions where performance was best for each method. Figure 5 shows a comparison between Jaccard distance for each animal, connecting lines indicate different methods performed on the same data segment, while each marker shape denotes a separate posture.

On average frequency filtering outperforms ensemble averaging based methods of perfusion calculation ($p=0.04$), and there is no significant difference in performance of the heart-frequency based filtering techniques during periods of apnoea relative to periods of ventilation.

Of the 56 data regions that were analysed, the ensemble averaging performed better in 12 cases and the frequency filtering achieved the best performance in 28 cases, there, were 16 additional cases where the difference in performance was negligible at less than 5%. On average, across all images, frequency filtering based methods scored 7% higher than ensemble averaging.

The center of mass of the perfusion measure images using the bolus injection method had a Cohen's d score of less than 0.1 between posture changes indicating that there is an insignificant or trivial difference in the means relative to the standard deviation (Cohen 1988). To demonstrate the visually observable changes due to posture change and the high similarities that can be observed between filtering- and bolus-based perfusion estimates, frequency filtered images from animal 4 are compared to bolus based methods in figure 6.

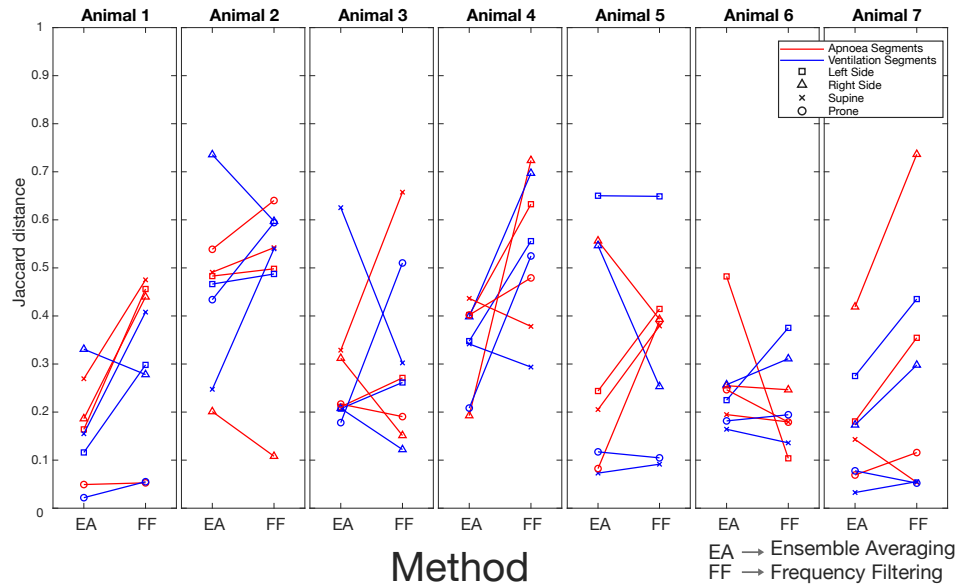


Figure 5. Jaccard scores for each method and animal in the comparison. Frequency filtering and ensemble averaging methods performed on the same data segment are connected by solid lines. Red lines and markers indicate apnoea data sections, while blue indicates ventilation data sections. Each posture is denoted by a different shaped marker in the figure.

4. Discussion

Two primary approaches of EIT perfusion calculation have been compared in this paper: injection of a bolus of contrast-agent resulting in EIT image changes which produce perfusion measures, and digital filtering of EIT image sequences to extract the heart-frequency components. Additionally, various algorithms have been evaluated for digital filtering-base approaches during mechanical ventilation and short apnoea sequences, using both frequency- and ensemble averaging-based techniques. There have been few comparisons of these techniques, and we set out to better understand the relationship between perfusion and heart-frequency measures, and between the various filtering approaches used to determine heart-frequency cardiac changes. We selected an experimental protocol using posture-change to alter the regional distribution of lung ventilation and perfusion in newborn lambs.

Our first question was “to what extent do heart-frequency filtering-based measures correspond to perfusion?”

The primary results (figure 5) use a Jaccard index of the similarity between functional images. Overall it was found that in healthy animals the Jaccard index indicated good agreement with our gold standard. While highly dependant on the data, it was found that there was a high degree of similarity between methods with respect to the overall shape of the perfusion. In both animals 2 and 4, where the signal required little preprocessing before analysis there is a higher Jaccard score across all cases.

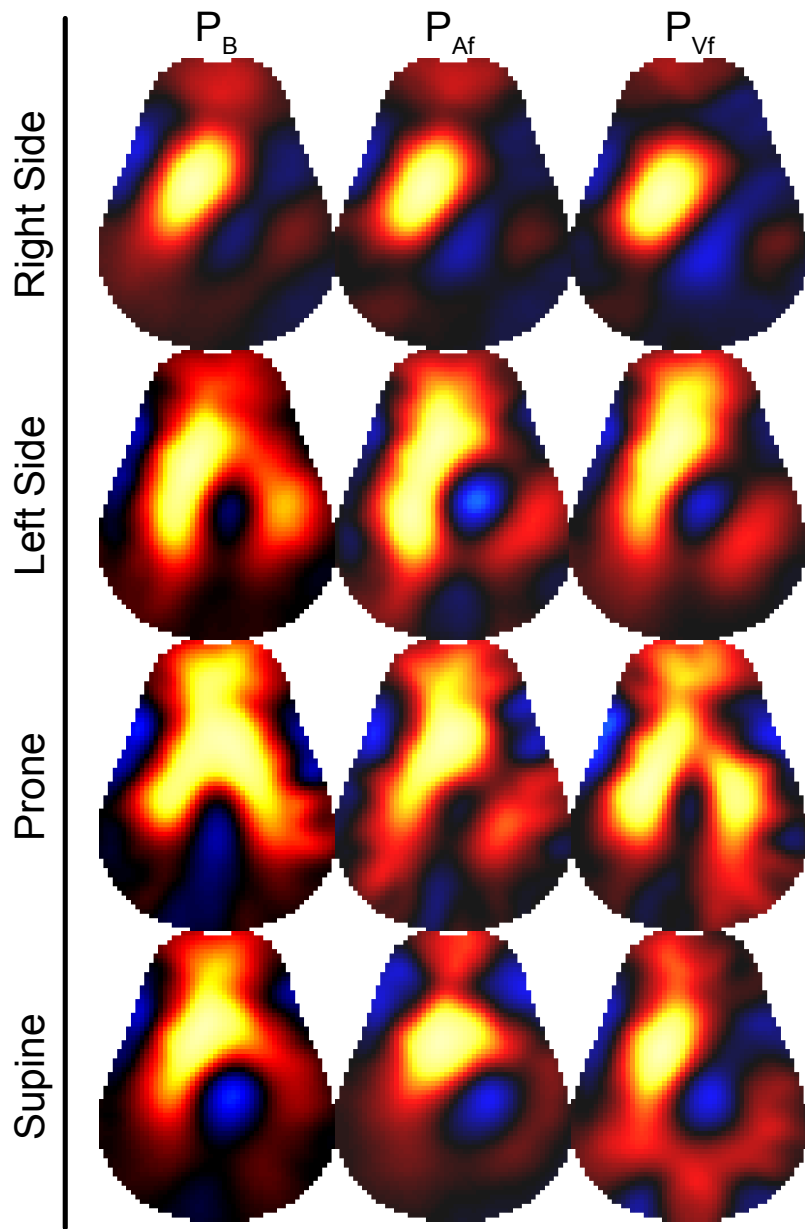


Figure 6. This figure shows the tracking of perfusion for frequency filtering measures of perfusion during apnoea and ventilation sections compared to bolus injection for animal 4. P_B is the bolus injection image, P_{Af} uses the frequency filtering method during apnoea and P_{Vf} is the frequency filtering method during ventilation.

The synchronisation box was attached to the EIT system but was not used for this experiment, an error in the connection caused brief periods of the signal (less than 1 s) in some animals to be zeroed. Through careful processing of this signal only brief sections of data were lost and we do not feel this impacts the results.

During the experiment the order of posture change was not randomised. While changes in ventilation due to posture change are not understood to have long term physiological effects, if there is a longer term effect of change in posture the lack of randomisation will impact the results. Nguyen *et al.* (2015) were able to image perfusion changes due to induced pulmonary embolisms and using the peak impedance change on dilution curves, however our data presented insufficient variance in perfusion induced by posture change to complete a center of mass analysis. A higher statistical power could potentially be achieved through initiating posture changes with more dramatic results in perfusion, such as upright to supine (Nakazato *et al.* 2010).

Throughout the experiment, the perfusion image was selected as the image containing the largest increase in conductivity in the sum of pixels in the lung region, which occurred at different relative times across animals and events. Many factors could affect this including belt positioning changes, and it could be a contributing factor to the inconsistent trends in amplitude changes in the global image across methods. Borges *et al.* (2012) compared EIT perfusion images using first-pass kinetics and heart-frequency filtering based methods to perfusion measures using SPECT, finding that heart-frequency filtering techniques made systemic errors when used to estimate the perfusion. They also determined that there was no discernible relationship between the magnitude of the SPECT images and the heart-frequency images. This was consistent with the findings of this study that image amplitude of the bolus injection and heart-frequency filtering-based methods was not consistent in all animals. This methodology presented by Borges *et al.* (2012) was not part of the comparison in this study as the identification of the perfusion signal due to the heart could not be consistently identified and removed across all animals. In two dimensions, heart-frequency and ventilation signals have been used to identify the location of the heart and lungs within the EIT electrode plane with known electrode locations and anatomy (Ferrario *et al.* 2012), but in situations where the electrode location and anatomy is not precisely known EIT tends to perform poorly as a structural imaging modality (Adler *et al.* 2017a). These challenges suggest that configurations with multiple planes of electrodes may be better able to isolate and remove off-plane pulsatility signals related to the heart.

It was observed that the general shape of the perfusion was consistent across all methods despite amplitude variations. One reason for the difference in amplitude change across animals may be due to slight variations in the belt placement and electrode positioning on the animals. If the belt is closer to the heart, there will be a larger heart-frequency component to the signal and there may be a variance in the impedance change due to bolus injection.

Next, we asked “what are the advantages and disadvantages of different approaches to heart-frequency filtering of EIT data, and which techniques are recommended under

which circumstances?"

Our overall recommendation is that, whenever possible, frequency filtering techniques should be used. This is largely because frequency filtering methods tend to be more stable in the presence of noise on the signal. Ensemble techniques are advantageous in some circumstances, because they better use the heart-frequency variability to avoid interference from harmonics of the ventilation at the heart rate. For frequency-filtering techniques, it is necessary to widen the heart-frequency filters to account for such variability. On the other hand, it is sometimes not possible to accurately synchronize heartbeats, due to noise corruption in the signals or the very low amplitude of the heart-frequency signals relative to the ventilation signal. In cases where the signal of the heartbeat was not clearly identifiable through visual inspection of the signal, neither ensemble averaging nor frequency filtering was able to achieve good estimates of perfusion relative to the bolus injection event.

In summary, our goal was to understand the relationship between bolus- and filtering-based EIT measurements of lung perfusion, as well as the relationship between different filtering-based measures of perfusion. Our results indicate there is a common trend between the shape and perfusion estimates of both heart-frequency and bolus injection images despite the difference in physiological events behind each measure. Amongst filtering techniques, frequency filtering outperforms ensemble averaging across regions of data where there is noise present and the heart signal cannot be readily identified, and both methods were able to approximate the bolus injection measures equally well when applied to apnoea and ventilation regions of data.

References

- Adler, A., Amato, M. B., Arnold, J. H., Bayford, R., Bodenstein, M., Böhm, S. H., Brown, B. H., Frerichs, I., Stenqvist, O., Weiler, N., & Wolf, G. K. (2012). Whither lung EIT: Where are we, where do we want to go and what do we need to get there? *Physiological Measurement*, 33(5), 679–694.
- Adler, A., Arnold, J. H., Bayford, R., Borsic, A., Brown, B., Dixon, P., Faes, T. J., Frerichs, I., Gagnon, H., Gärber, Y., Grychtol, B., Hahn, G., Lionheart, W. R., Malik, A., Patterson, R. P., Stocks, J., Tizzard, A., Weiler, N., & Wolf, G. K. (2009). GREIT: A unified approach to 2D linear EIT reconstruction of lung images. *Physiological Measurement*, 30(6), S35–55.
- Adler, A., & Boyle, A. (2017a). Electrical impedance tomography: Tissue properties to image measures. *IEEE Transactions on Biomedical Engineering*, 64(11), 2494–2504.
- Adler, A., Boyle, A., Braun, F., Crabb, M. G., Grychtol, B., Lionheart, W. R. B., Tregidgo, H. F. J., & Yerworth, R. (2017b). EIDORS Version 3.9. In *International conference on biomedical applications of electrical impedance tomography*.

- Bartocci, M., Serra, G., Basano, L., Canepa, F., & Ottonello, P. (1999). Cerebral blood-flow monitor for use in neonatal intensive care units. *Computer Methods and Programs in Biomedicine*, 59(1), 61–73.
- Bhuyan, U., Peters, A. M., Gordon, I., Davies, H., & Helms, P. (1989). Effects of posture on the distribution of pulmonary ventilation and perfusion in children and adults. *Thorax*, 44(6), 480–484.
- Borges, J. B., Suarez-Sipmann, F., Bohm, S. H., Tusman, G., Melo, A., Maripuu, E., Sandström, M., Park, M., Costa, E. L. V., Hedenstierna, G., & Amato, M. (2012). Regional lung perfusion estimated by electrical impedance tomography in a piglet model of lung collapse. *Journal of Applied Physiology*, 112(1), 225–236.
- Braun, F., Proença, M., Adler, A., Riedel, T., Thiran, J. P., & Solà, J. (2018). Accuracy and reliability of noninvasive stroke volume monitoring via ECG-gated 3D electrical impedance tomography in healthy volunteers. *PLoS ONE*, 13(1), 1–19.
- Cohen, J. (1988). *Statistical Power Analysis for the Behavioral Sciences* (Second Edi). Hillsdale, N.J: Lawrence Erlbaum Associates.
- Deibele, J. M., Luepschen, H., & Leonhardt, S. (2008). Dynamic separation of pulmonary and cardiac changes in electrical impedance tomography. *Physiological Measurement*, 29(6), S1–S14.
- Ericsson, E., Tesselaar, E., & Sjöberg, F. (2016). Effect of electrode belt and body positions on regional pulmonary ventilation- and perfusion-related impedance changes measured by electric impedance tomography. *PLoS ONE*, 11(6), 1–14.
- Eyüboğlu, B. M., Brown, B. H., & Barber, I. D. (1989). In Vivo Imaging of Cardiac Related Impedance Changes. *IEEE Engineering in Medicine and Biology Magazine*, 8(1), 39–45.
- Ferrario, D., Grychtol, B., Adler, A., Sola, J., Bohm, S. H., & Bodenstein, M. (2012). Toward morphological thoracic EIT: Major signal sources correspond to respective organ locations in CT. *IEEE Transactions on Biomedical Engineering*, 59(11 PART1), 3000–3008.
- Frerichs, I., Hinz, J., Herrmann, P., Weisser, G., Hahn, G., Quintel, M., & Hellige, G. (2002). Regional lung perfusion as determined by electrical impedance tomography in comparison with electron beam CT imaging. *IEEE Transactions on Medical Imaging*, 21(6), 646–652.
- Frerichs, I., Amato, M. B., Van Kaam, A. H., Tingay, D. G., Zhao, Z., Grychtol, B., Bodenstein, M., Gagnon, H., Böhm, S. H., Teschner, E., Stenqvist, O., Mauri, T., Torsani, V., Camporota, L., Schibler, A., Wolf, G. K., Gommers, D., Leonhardt, S., Adler, A., Fan, E., Lionheart, W. R., Riedel, T., Rimensberger, P. C., Sipmann, F. S., Weiler, N., & Wrigge, H. (2017). Chest electrical impedance tomography examination, data analysis, terminology, clinical use and recommendations: Consensus statement of the TRanslational EIT developmeNt stuDy group. *Thorax*, 72(1), 83–93.

- Grychtol, B., Müller, B., & Adler, A. (2016). 3D EIT image reconstruction with GREIT. *Physiological Measurement*, 37(6), 785–800.
- Halter, R. J., Hartov, a., & Paulsen, K. D. (2008). Imaging forearm blood flow with pulse-ox gated electrical impedance tomography. *Conference proceedings : ... Annual International Conference of the IEEE Engineering in Medicine and Biology Society. IEEE Engineering in Medicine and Biology Society. Conference, 2008*, 1192–5.
- Leathard, A. D., Brown, B. H., Campbell, J., Zhang, F., Morice, A. H., & Tayler, D. (1994). A comparison of ventilatory and cardiac related changes in EIT images of normal human lungs and of lungs with pulmonary emboli. *Physiological Measurement*, 15(2A), 137–146.
- Leonhardt, S., & Lachmann, B. (2012). Electrical impedance tomography: The holy grail of ventilation and perfusion monitoring? *Intensive Care Medicine*, 38(12), 1917–1929.
- Moens, Y., Schramel, J. P., Tusman, G., Ambrisko, T. D., Solà, J., Brunner, J. X., Kowalczyk, L., & Böhm, S. H. (2014). Variety of non-invasive continuous monitoring methodologies including electrical impedance tomography provides novel insights into the physiology of lung collapse and recruitment - case report of an anaesthetized horse. *Veterinary Anaesthesia and Analgesia*, 41(2), 196–204.
- Nakazato, R., Tamarappoo, B. K., Kang, X., Wolak, A., Kite, F., Hayes, S. W., Thomson, L. E. J., Friedman, J. D., Berman, D. S., & Slomka, P. J. (2010). Quantitative Upright-Supine High-Speed SPECT Myocardial Perfusion Imaging for Detection of Coronary Artery Disease: Correlation with Invasive Coronary Angiography. *Journal of Nuclear Medicine*, 51(11), 1724–1731.
- Nguyen, D. T., Jin, C., Thiagalingam, A., & Mcewan, A. L. (2012). A review on electrical impedance tomography for pulmonary perfusion imaging. *Physiological Measurement*, 33(5), 695–706.
- Nguyen, D. T., Bhaskaran, A., Hospital, W., Chik, W., Anthony, M., & Barry, T. (2015). Perfusion redistribution after a pulmonary-embolism-like event with contrast enhanced EIT. *Physiological Measurement*, 36(6), 1297–1309.
- Proença, M., Braun, F., Solà, J., Thiran, J. P., & Lemay, M. (2017). Noninvasive pulmonary artery pressure monitoring by EIT: a model-based feasibility study. *Medical and Biological Engineering and Computing*, 55(6), 949–963.
- Reifferscheid, F., Elke, G., Pulletz, S., Gawelczyk, B., Lautenschläger, I., Steinfath, M., Weiler, N., & Frerichs, I. (2011). Regional ventilation distribution determined by electrical impedance tomography: Reproducibility and effects of posture and chest planerresp. *Respirology*, 16(3), 523–531.
- Sage, M., Nadeau, M., Forand-Choinière, C., Mousseau, J., Vandamme, J., Berger, C., Tremblay-Roy, J. S., Tissier, R., Micheau, P., & Fortin-Pellerin, É. (2018). Assessing the impacts of total liquid ventilation on left ventricular diastolic function in a model of neonatal respiratory distress syndrome. *PLoS ONE*, 13(1), 1–11.

- Solà, J., Adler, A., Santos, A., Tusman, G., Sipmann, F. S., & Bohm, S. H. (2011). Non-invasive monitoring of central blood pressure by electrical impedance tomography: First experimental evidence. *Medical and Biological Engineering and Computing*, 49(4), 409–415.
- Xue, F. S., Luo, L. K., Tong, S. Y., Liao, X., Deng, X. M., & An, G. (1996). Study of the Safe Threshold of Apneic Period in Children during Anesthesia Induction. *Journal of Clinical Anesthesia*, 8(7), 568–574.
- Zadehkoochak, M., Blott, B. H., Harrtest, T. K., & Georget, R. F. (1992). Pulmonary Perfusion and Ventricular Ejection Imaging by Frequency Domain Filtering of Eit Images. *Clinical Physics and Physiological Measurement*, 13(1990), 191–196.